

**A parametric study for the generation of ion Bernstein modes from a discrete spectrum to a continuous one in the inner magnetosphere. I. Linear theory**

Jicheng Sun, Xinliang Gao, Lunjin Chen, Quanming Lu, Xin Tao, and Shui Wang

Citation: *Physics of Plasmas* **23**, 022901 (2016); doi: 10.1063/1.4941283

View online: <http://dx.doi.org/10.1063/1.4941283>

View Table of Contents: <http://scitation.aip.org/content/aip/journal/pop/23/2?ver=pdfcov>

Published by the **AIP Publishing**

---

**Articles you may be interested in**

[A parametric study for the generation of ion Bernstein modes from a discrete spectrum to a continuous one in the inner magnetosphere. II. Particle-in-cell simulations](#)

*Phys. Plasmas* **23**, 022902 (2016); 10.1063/1.4941284

[Resonance zones for electron interaction with plasma waves in the Earth's dipole magnetosphere. I. Evaluation for field-aligned chorus, hiss, and electromagnetic ion cyclotron waves](#)

*Phys. Plasmas* **17**, 042902 (2010); 10.1063/1.3310834

[Bernstein mode generated anomalous resistivity in a current carrying plasma focusing cell](#)

*Phys. Plasmas* **13**, 103106 (2006); 10.1063/1.2357048

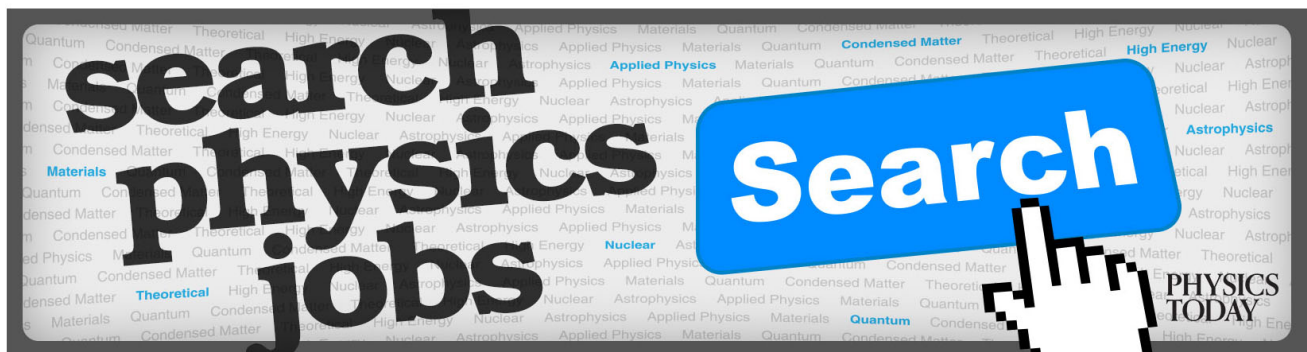
[Electron Bernstein wave generation in a linear plasma system](#)

*Phys. Plasmas* **11**, 4582 (2004); 10.1063/1.1784787

[Collective phenomena in the inner magnetosphere](#)

*Phys. Plasmas* **6**, 4195 (1999); 10.1063/1.873685

---



# A parametric study for the generation of ion Bernstein modes from a discrete spectrum to a continuous one in the inner magnetosphere. I. Linear theory

Jicheng Sun,<sup>1,2</sup> Xinliang Gao,<sup>1,2,a)</sup> Lunjin Chen,<sup>3</sup> Quanming Lu,<sup>1,2</sup> Xin Tao,<sup>1,2</sup> and Shui Wang<sup>1,2</sup>

<sup>1</sup>CAS Key Laboratory of Geospace Environment, Department of Geophysics and Planetary Science, University of Science and Technology of China, Hefei 230026, China

<sup>2</sup>Collaborative Innovation Center of Astronautical Science and Technology, Harbin 150001, China

<sup>3</sup>Department of Physics, University of Texas at Dallas, Richardson, Texas 75080-3021, USA

(Received 9 November 2015; accepted 20 January 2016; published online 10 February 2016)

Ion Bernstein modes, also known as magnetosonic waves in the magnetospheric community, are considered to play an important role in radiation belt electron acceleration. The detailed properties of perpendicular magnetosonic waves excited in the inner magnetosphere by a tenuous proton ring distribution are investigated in a two series paper with a combination of the linear theory and one-dimensional particle-in-cell simulations. Here, in this paper, we study the properties of the excited magnetosonic waves under different plasma conditions with the linear theory. When the proton to electron mass ratio or the ratio of the light speed to the Alfvén speed is small, the excited magnetosonic waves are prone to having a discrete spectrum with only several wave modes. With the increase of the proton to electron mass ratio or the ratio of the light speed to the Alfvén speed, the lower hybrid frequency also increases, which leads to the increase of both the number and frequency of the excited wave modes. Meanwhile, the growth rate of these wave modes also increases. When the proton to electron mass ratio or the ratio of the light speed to the Alfvén speed is sufficiently large, the spectrum of the excited magnetic waves becomes continuous due to the overlapping of the adjacent wave modes. The increase of the density of the protons with the ring distribution can also result in the increase of the growth rate, which may also change the discrete spectrum of the excited waves to a continuous one, while the increase of the ring velocity of the tenuous proton ring distribution leads to a broader spectrum, but with a smaller growth rate.

© 2016 AIP Publishing LLC. [<http://dx.doi.org/10.1063/1.4941283>]

## I. INTRODUCTION

Ion Bernstein modes in the magnetosphere, which are also called equatorial noises or fast magnetosonic waves, are frequently observed within  $2^\circ$ – $3^\circ$  of the geomagnetic equator at the radial distance from  $L = 2$  to 8.<sup>1–4</sup> Those three terms will be used interchangeably throughout the manuscript. The bulk of the fast magnetosonic mode observation are within  $\pm 3^\circ$  or so of the magnetic equator, with a tail extending to higher latitudes.<sup>5–10</sup> The wave vector of this mode is nearly perpendicular to the background magnetic field, whose frequencies range from the proton cyclotron frequency to the lower hybrid frequency.<sup>11–13</sup> Recently, these enhanced fluctuations have received increased attention because of their potential role in the radiation belt electron acceleration.<sup>14,15</sup>

Satellite observations<sup>2,16–18</sup> have shown that magnetosonic waves in the inner magnetosphere are closely associated with a tenuous energetic proton ring-like distribution with  $\partial f_h(v_\perp)/\partial v_\perp > 0$  (where  $f_h(v_\perp)$  is the perpendicular velocity distribution function of energetic protons) in the presence of a cold dense background plasma, and theoretical calculations<sup>16,19–23</sup> found that such a distribution is unstable to magnetosonic waves when the ring velocity  $V_R$  is comparable to  $V_A$  (where  $V_A$  is the Alfvén velocity). Simultaneously, both observations and theoretical results have demonstrated that

these waves occur at the harmonics of the proton gyrofrequency up to the lower hybrid frequency. These observations support that magnetosonic waves in the inner magnetosphere are driven by the ring-like distribution of energetic protons.

Recently, particle-in-cell (PIC) simulations<sup>24</sup> have been performed to study magnetosonic waves driven by a proton velocity distribution with a positive slope in the perpendicular velocity distribution, and the excited waves have the characteristics consistent with the linear theory: their frequencies are ranging from the proton cyclotron frequency to the lower hybrid frequency, and the wave vector is nearly perpendicular to the background magnetic field. In addition, both observations and the linear theory have shown that magnetosonic waves have a discrete spectrum, where the waves are emitted at frequencies corresponding to exact multiples of the proton gyrofrequency. However, the excited magnetosonic waves in the previous PIC simulations usually only have several harmonics due to the reduced ratio of both the proton mass to electron mass and light speed to Alfvén speed,<sup>24</sup> while both the observations and linear theory have shown that magnetosonic waves have tens of discrete emission lines.<sup>13,19</sup> Moreover, the POLAR observations by Tsurutani *et al.*<sup>10</sup> have reported that magnetosonic waves can also have a continuous spectrum. The observation of the continuous spectrum is interesting. In addition to propagation effects that might blur discrete emissions, Chen<sup>25</sup> shows that the proton ring distribution is capable of generating ion

<sup>a)</sup>Author to whom correspondence should be addressed. Electronic mail: [gaoxl@mail.ustc.edu.cn](mailto:gaoxl@mail.ustc.edu.cn)

Bernstein modes over a continuous spectrum too, which could be another possible explanation.

It is worthy exploring the regimes for the continuous or discrete spectrum generation using both linear theory and PIC simulations. The goal of this series of two papers is to investigate the different spectra of the perpendicular magnetosonic waves excited by the tenuous energetic proton ring-like distribution in the presence of a cold dense background plasma under different plasma conditions. The parameters under exploration include several physical parameters and two artificial parameters often used in PIC simulation, i.e., the mass ratio  $m_h/m_e$  and the velocity ratio  $c/V_A$ . In this paper, we discuss in detail the spectral properties of magnetosonic waves with the linear theory. Then, one-dimensional (1-D) PIC simulations are performed with the similar plasma conditions [hereafter referred to as Paper II<sup>26</sup>] to figure out the factors to determine the spectrum of magnetosonic waves, and further study the particle dynamics.

The paper is organized as follows. The theoretical model is described in Sec. II, and the results are presented in Sec. III. In Sec. IV, we give a conclusion, which is followed by the discussions.

## II. THEORETICAL MODEL

In this paper, we assume a uniform and magnetized plasma consisting of three components: cold electrons, cold protons, and ring distribution protons. Their number densities are  $n_e$ ,  $n_{hc}$ , and  $n_{hr}$ , respectively. To satisfy the charge neutrality, it requires  $n_e = n_{hc} + n_{hr}$ . The distribution function of ring distribution protons is  $f_{hr} = n_{hr} \delta(v_{\parallel}) \delta(v_{\perp} - V_R) / (2\pi v_{\perp})$ , where  $v_{\parallel}$  and  $v_{\perp}$  are velocities parallel and perpendicular to the background magnetic field  $\mathbf{B}_0 = B_0 \mathbf{e}_y$ , and  $V_R$  is the proton ring velocity.

Because the wave vector of the magnetosonic waves is nearly perpendicular to the background magnetic field, in this paper for simplicity, we assume that the wave vector of the magnetosonic waves is perpendicular to the background magnetic field. In such a situation, the dispersion relation of magnetosonic waves can be expressed as

$$D(\omega, k) = \varepsilon_{xx}(\varepsilon_{zz} - n^2) + \varepsilon_{xz}^2 = 0, \quad (1)$$

TABLE I. Parameters for different cases.

| Case | $V_R/V_A$ | $n_{hr}/n_e$ (%) | $c/V_A$ | $m_h/m_e$ |
|------|-----------|------------------|---------|-----------|
| 1    | 1         | 0.5              | 138     | 100       |
| 2    | 1         | 0.5              | 138     | 400       |
| 3    | 1         | 0.5              | 138     | 900       |
| 4    | 1         | 0.5              | 138     | 1600      |
| 5    | 1         | 0.5              | 10      | 1600      |
| 6    | 1         | 0.5              | 20      | 1600      |
| 7    | 1         | 0.5              | 50      | 1600      |
| 8    | 1         | 0.5              | 20      | 400       |
| 9    | 1         | 1.0              | 20      | 400       |
| 10   | 1         | 2.0              | 20      | 400       |
| 11   | 0.7       | 0.5              | 50      | 900       |
| 12   | 1         | 0.5              | 50      | 900       |
| 13   | 1.3       | 0.5              | 50      | 900       |

where the refractive index is  $n = kc/\omega$ ,  $\omega$  is the complex frequency, and  $k$  is the perpendicular wave number.  $\varepsilon_{xx}$ ,  $\varepsilon_{zz}$ ,  $\varepsilon_{xz}$  are elements of the dielectric tensor  $\varepsilon$ . The subscript  $x$  denotes the direction of the wave vector  $\mathbf{k}$ , and the background magnetic field  $\mathbf{B}_0$  is along  $y$  axis.

The dielectric tensor elements are found to be

$$\begin{aligned} \varepsilon_{xx} &= 1 + \frac{\omega_{pe}^2}{\Omega_e^2 - \omega^2} + \frac{\omega_{phc}^2}{\Omega_h^2 - \omega^2} + \frac{\omega_{phr}^2}{\omega^2} \\ &\quad \times \left( -1 + \sum_n \frac{n2n^2 J_n(t) J'_n(t)}{n - \omega/\Omega_h} \right), \\ \varepsilon_{xz} &= \frac{i\omega_{pe}^2 \Omega_e}{(\Omega_e^2 - \omega^2)\omega} + \frac{i\omega_{phc}^2 \Omega_h}{(\Omega_h^2 - \omega^2)\omega} \\ &\quad + \frac{\omega_{phr}^2}{\omega^2} \sum_n \frac{in^2 [J'_n(t)^2 + J_n(t) J'_n(t)/t + J_n(t) J''_n(t)]}{n - \omega/\Omega_h}, \\ \varepsilon_{zz} &= 1 + \frac{\omega_{pe}^2}{\Omega_e^2 - \omega^2} + \frac{\omega_{phc}^2}{\Omega_h^2 - \omega^2} \\ &\quad + \frac{\omega_{phr}^2}{\omega^2} \left( -1 + \sum_n \frac{n2J'_n(t)(J'_n(t) + tJ''_n(t))}{n - \omega/\Omega_h} \right), \end{aligned} \quad (2)$$

where the electron cyclotron frequency is  $\Omega_e = -eB_0/m_e$ , the proton cyclotron frequency is  $\Omega_h = eB_0/m_h$ , the electron plasma frequency is  $\omega_{pe} = \sqrt{n_e e^2 / (\varepsilon_0 m_e)}$ , and the proton plasma frequencies for cold and ring distribution components are  $\omega_{ph} = \sqrt{n_{hc} e^2 / (\varepsilon_0 m_h)}$  and  $\omega_{phr} = \sqrt{n_{hr} e^2 / (\varepsilon_0 m_h)}$  (where  $\varepsilon_0$  is vacuum permittivity,  $e$  is elementary charge, and  $m_e$  and  $m_h$  are electron and proton masses, respectively).  $J_n$  denotes Bessel functions with argument  $t = kV_R/\Omega_h$ . The dispersion relation (Eq. (1)) will be solved to obtain the complex frequency  $\omega$  under given plasma parameters, whose real part is the real wave frequency  $\omega_r$  and imaginary part is the temporal growth rate  $\gamma$ . There are multiple solutions of the complex frequency for a given  $k$ . To find unstable modes with  $\gamma > 0$ , we will search all possible unstable solutions for a given  $k$  in the complex frequency domain with  $1.5 \leq \omega_r/\Omega_h \leq 40$  and  $10^{-3} \leq \gamma/\Omega_h \leq 1$ . Such a root finding procedure is repeated for each  $k$  from  $0.1k_0$  to  $50k_0$  with a spacing  $0.02k_0$  (where  $k_0$  is  $\Omega_h/V_A$ , and  $V_A$  is the Alfvén speed). In this way, we can ensure that all the complex frequency solutions within the domain will be identified for a given  $k$ .

## III. RESULTS

In this paper, we present the spectral characteristics of magnetosonic waves excited by a tenuous proton ring distribution under different plasma conditions. PIC simulations of magnetosonic waves usually use a reduced mass ratio of proton to electron and a reduced ratio of the light speed to the Alfvén speed in order to save computational source.<sup>24</sup> In this paper, we will compare the spectral characteristics of magnetosonic waves with different mass ratios and ratios of the light speed to the Alfvén speed, as well as the number density and ring velocity of the ring distribution protons. The parameters for different calculations are listed in Table I. In the following, we describe the theoretical results in detail.

In the inner magnetosphere, the background magnetic field  $B_0$  is about 100 nT, and the electron number density  $n_e$  is about  $1 \text{ cm}^{-3}$ . Then, the Alfvén speed is  $V_A \sim 2.18 \times 10^3 \text{ km/s}$ , and  $c/V_A$  is about 138. First, we investigate the effects of the mass ratio on the spectral characteristics of magnetosonic waves by keeping  $n_{hr}/n_e = 0.5\%$ ,  $V_R = 1.0V_A$ , and  $c/V_A = 138$ . Figure 1 shows the dispersion relation of perpendicular magnetosonic waves for different proton-to-electron mass ratios (cases 1–4). Figure 1(a) presents the normalized wave frequency  $\omega_r/\Omega_h$  versus the normalized wave number  $k/k_0$  (left panels), and Figure 1(b) presents the normalized wave frequency  $\omega_r/\Omega_h$  versus the normalized growth rate  $\gamma/\Omega_h$  (right panels) for  $m_h/m_e = 100$ , Figures 1(c) and 1(d) for  $m_h/m_e = 400$ , Figures 1(e) and 1(f) for  $m_h/m_e = 900$ , and Figures 1(g) and 1(h) for  $m_h/m_e = 1600$ . When the mass ratio is small, for example,  $m_h/m_e = 100$ , only several discrete wave modes with the harmonics of the proton gyrofrequency are excited. With the increase of the mass ratio, more wave modes are excited.

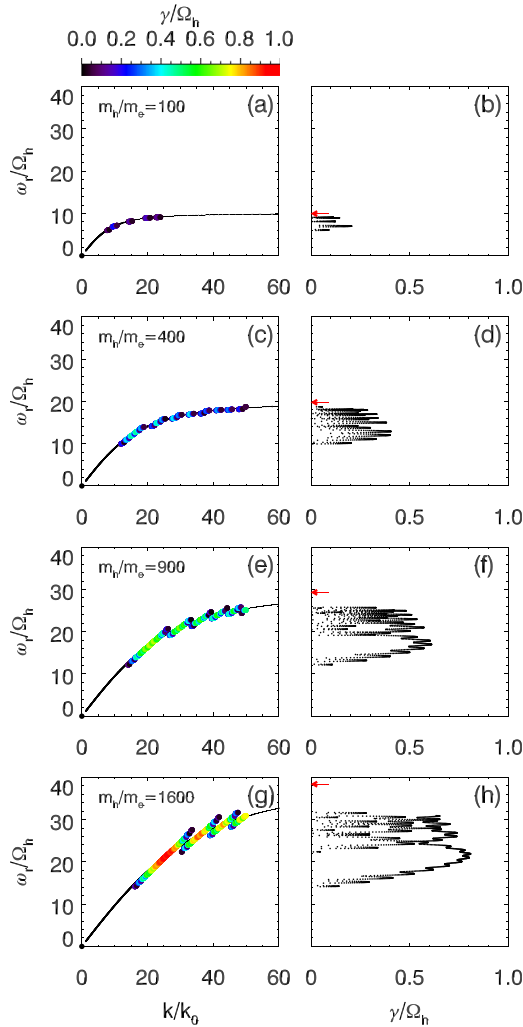


FIG. 1. (a) The normalized wave frequency  $\omega_r/\Omega_h$  versus the normalized wave number  $k/k_0$ , and (b) the normalized wave frequency  $\omega_r/\Omega_h$  versus the normalized growth rate  $\gamma/\Omega_h$  for case 1, while (c) and (d) for case 2, (e) and (f) for case 3, and (g) and (h) for case 4. The black lines in left panel represent the cold plasma dispersion relation. Colored line segments denote unstable wave modes, with red for greater  $\gamma$  and blue for smaller  $\gamma$  values. The red arrows in right panels mark the lower hybrid frequency.

Simultaneously, the frequencies of the several dominant modes (with a relatively larger growth rate) become larger, and the spectral range of the excited waves becomes broader. For example, the frequencies are about from  $6\Omega_h$  to  $9\Omega_h$  when the mass ratio  $m_h/m_e$  is 100, while the frequencies are about from  $14\Omega_h$  to  $32\Omega_h$  when the mass ratio  $m_h/m_e$  is 1600. These results can be explained by the increase of the lower hybrid frequency with the increase of the mass ratio. The lower hybrid resonant frequency  $\Omega_{lh}$  can be obtained through

$$\frac{1}{\Omega_{lh}^2} = \frac{1}{\Omega_e \Omega_h} + \frac{1}{\omega_{ph}^2} = \left( \frac{m_e}{m_h} + \left( \frac{V_A}{c} \right)^2 \right) \frac{1}{\Omega_h^2}. \quad (3)$$

One can see that for a fixed  $c/V_A$ ,  $\Omega_{lh}$  increases with the increase of the mass ratio  $m_h/m_e$  (red arrows in Fig. 1). Because the excited magnetosonic waves have frequencies from the proton gyrofrequency to the lower hybrid frequency, it is easy to imagine that the spectral range of the excited magnetosonic waves will become broader and their dominant modes will have larger frequencies with the increasing mass ratio  $m_h/m_e$ .

We can also find that the growth rate of these waves increases with the increase of the mass ratio. Usually, the frequency width of one growth rate peak is on the order of its corresponding peak growth rate.<sup>19,25</sup> Hence, when the mass ratio is small, the frequency width for each peak at the harmonics of the proton cyclotron frequency is small, and there is a power gap between the adjacent peaks. However, when the mass ratio becomes larger, the growth peak has a larger frequency width because of their larger growth rate. This leads to the overlapping between two adjacent wave modes, and then a continuous spectrum of the waves is formed due to the merging of growth rate peaks when the mass ratio is sufficiently large (for example,  $m_h/m_e = 900$  and 1600). It is expected that PIC simulations with unrealistic low  $m_h/m_e$  (to reduce computation cost) tend to inhibit the merging of neighboring wave modes into a continuous spectrum.

The effects of the ratio of the light speed to Alfvén speed on the spectral properties of excited magnetosonic waves are also considered in this paper. Figure 2 shows the dispersion relation of perpendicular magnetosonic waves for different ratios of the light speed to Alfvén speed (cases 5–7), while  $n_{hr}/n_e = 0.5\%$ ,  $V_R = 1.0V_A$ , and  $m_h/m_e = 1600$  are kept. Figure 2(a) shows the normalized wave frequency  $\omega_r/\Omega_h$  versus the normalized wave number  $k/k_0$  (left panels), and Figure 2(b) shows the normalized wave frequency  $\omega_r/\Omega_h$  versus the normalized growth rate  $\gamma/\Omega_h$  (right panels) for  $c/V_A = 10$ , Figures 2(c) and 2(d) for  $c/V_A = 20$ , Figures 2(e) and 2(f) for  $c/V_A = 50$ , and Figures 2(g) and 2(h) for  $c/V_A = 138$ . Similar to the results with the increase of the mass ratio, when the light speed is small, only several discrete wave modes are excited. With the increase of the ratio of the light speed to the Alfvén speed, the excited magnetosonic waves have larger frequencies and a broader spectrum. This can also be explained by the increase of the lower hybrid frequency with the increase of the light speed (see Eq. (3)). At the same time, the increase of the light speed can

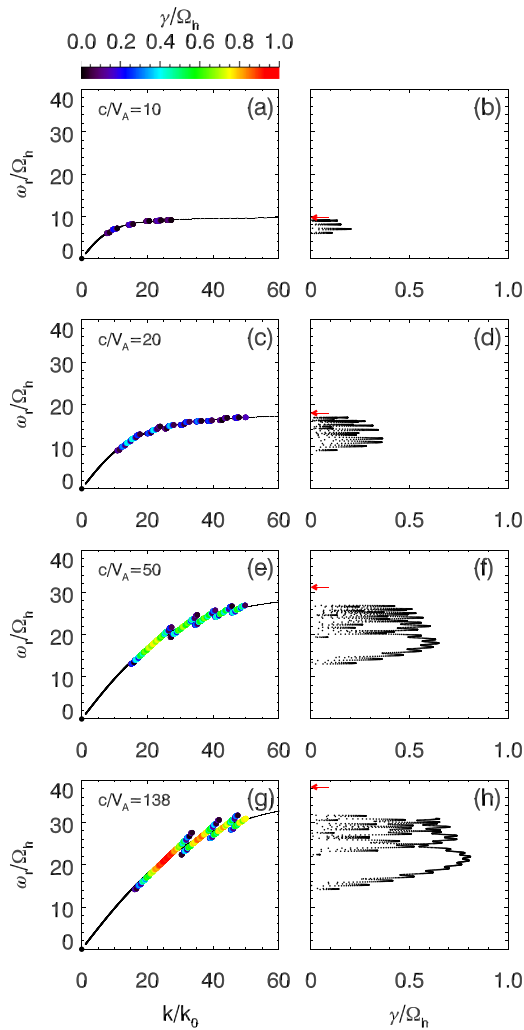


FIG. 2. (a) The normalized wave frequency  $\omega_r/\Omega_h$  versus the normalized wave number  $k/k_0$ , and (b) the normalized wave frequency  $\omega_r/\Omega_h$  versus the normalized growth rate  $\gamma/\Omega_h$  for case 5, while (c) and (d) for case 6, (e) and (f) for case 7, and (g) and (h) for case 4. The black lines in left panel represent the cold plasma dispersion relation. Colored line segments denote unstable wave modes, with red for greater  $\gamma$  and blue for smaller  $\gamma$  values. The red arrows in right panels mark the lower hybrid frequency.

also lead to the increase of the growth rate as well as the frequency width of each growth peak, which causes the peaks of the discrete growth rate to overlap with each other. Therefore, the discrete modes will merge into a continuous spectrum when the ratio of the light speed to the Alfvén speed is sufficiently large (for example, when  $c/V_A = 50$  and 138). PIC simulations that use reduced  $c/V_A$  to lower computation cost will likely fail to capture the formation of the continuous spectrum.

Obviously, the properties of the excited magnetosonic waves change significantly with the different  $m_h/m_e$  and  $c/V_A$ , since the spectrum may become continuous from a discrete one with higher  $m_h/m_e$  and  $c/V_A$ . To show more clearly the conditions where a continuous spectrum can be formed, we explore artificial effects of PIC simulations over a range of the light to Alfvén speed ratio from 10 to 138 and over a range of the proton to electron mass ratio from 16 to 1600, keeping  $n_{hr}/n_e = 0.5\%$  and  $V_R/V_A = 1$ . Then, we sort the resultant spectra into the two categories, discrete and

continuous, which are shown as blue dots and red dots, respectively, in Fig. 3. One can see a clear trend that continuous spectrum formation favors higher  $m_h/m_e$  and higher  $c/V_A$ , which are more realistic values. When  $m_h/m_e$  is 900, the spectrum becomes continuous when  $c/V_A$  is larger than 50. When  $m_h/m_e$  is 1600,  $c/V_A \geq 30$  is the condition, where the spectrum becomes continuous. It is important to note unrealistic lower values of  $m_h/m_e$  and  $c/V_A$  used in PIC simulations might not give realistic representation of the discrete/continuous spectrum, in addition to limitations of the numbers of discrete emissions. For example, the parameters adopted by the PIC simulation from Ref. 24,  $m_h/m_e = 900$  and  $c/V_A = 15$  (shown as a green plus symbol in Fig. 3), are less likely to explore the formation of the continuous spectrum.

Figure 4 shows the dispersion relation of perpendicular magnetosonic waves for different number densities of the ring distribution protons (cases 8–10), while  $V_R = 1.0V_A$ ,  $c/V_A = 20$ , and  $m_h/m_e = 400$  are kept. Figure 4(a) plots the normalized wave frequency  $\omega_r/\Omega_h$  versus the normalized wave number  $k/k_0$  (left panels), and Figure 4(b) exhibits the normalized wave frequency  $\omega_r/\Omega_h$  versus the normalized growth rate  $\gamma/\Omega_h$  (right panels) for  $n_{hr}/n_e = 0.5\%$ , Figures 4(c) and 4(d) for  $n_{hr}/n_e = 1\%$  and Figures 4(e) and 4(f) for  $n_{hr}/n_e = 2\%$ . With the increase of the number density of the ring distribution protons, there is no obvious change for the spectral range of the excited waves. However, the growth rate of excited magnetosonic waves increases, because there is more free energy when the number density of the ring distribution proton increases. Then, it is easy to understand when the number density of the ring distribution proton is sufficiently large, the spectrum of the excited waves will change from a discrete spectrum to a continuous one. It is also due to the merging of growth rate peaks, because both the growth rate and frequency width for each peak at the harmonics of proton cyclotron frequency increase with the increase of the number density of the ring distribution proton. Figure 5 shows the spectral properties of the excited magnetosonic waves at different ratios of the light speed to

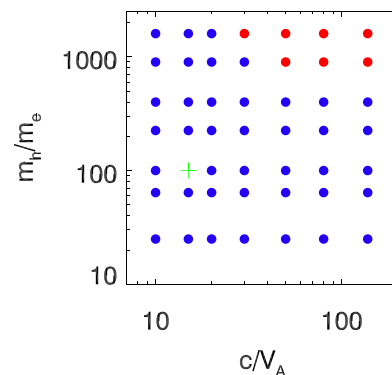


FIG. 3. The spectral properties of excited magnetosonic waves at different ratios of the light speed to the Alfvén speed  $c/V_A$  and mass ratios of proton to electron  $m_h/m_e$ , while  $n_{hr}/n_e$  and  $V_R$  are kept as 0.5% and  $1.0V_A$ , respectively. Each dot denotes one case. The red and blue colors represent a continuous spectrum and a discrete spectrum of magnetosonic waves, respectively. The green pulse symbol represents the combined parameters,  $m_h/m_e = 900$  and  $c/V_A = 20$ , used by Liu *et al.*<sup>24</sup>

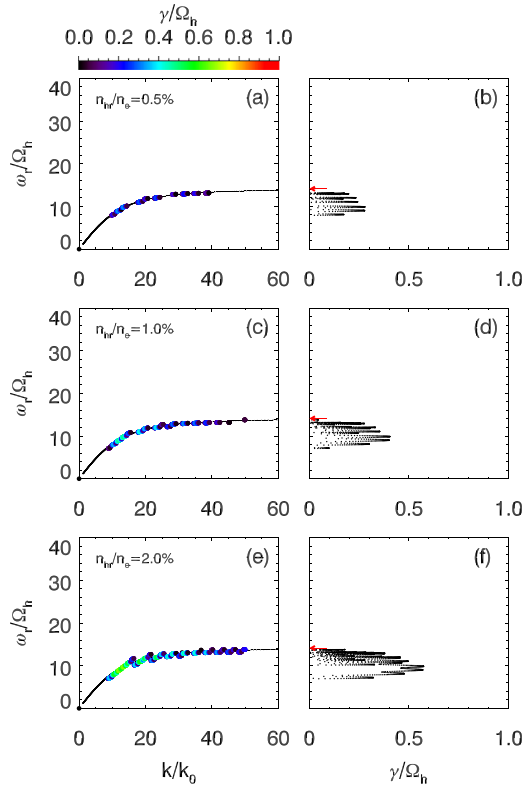


FIG. 4. (a) The normalized wave frequency  $\omega_r/\Omega_h$  versus the normalized wave number  $k/k_0$ , and (b) the normalized wave frequency  $\omega_r/\Omega_h$  versus the normalized growth rate  $\gamma/\Omega_h$  for case 8, while (c) and (d) for case 9, and (e) and (f) for case 10. The black lines in left panel represent the cold plasma dispersion relation. Colored line segments denote unstable wave modes, with red for greater  $\gamma$  and blue for smaller  $\gamma$  values. The red arrows in right panels mark the lower hybrid frequency.

the Alfvén speed and mass ratios of proton to electron, for  $n_{hr}/n_e = 1\%$  (Fig. 5(a)) and for  $n_{hr}/n_e = 2\%$  (Fig. 5(b)) while  $V_R$  is kept as  $1.0V_A$ . Similar to the case of  $n_{hr}/n_e = 0.5\%$  (Fig. 3), continuous spectrum formation favors high  $m_h/m_e$  and high  $c/V_A$ . The difference is that the larger number density of the ring distribution protons lowers the thresholds for  $m_h/m_e$  and  $c/V_A$  for the continuous spectrum formation. When  $n_{hr}/n_e = 2\%$ , a continuous spectrum can even be formed at  $m_h/m_e = 200$  and  $c/V_A = 20$ .

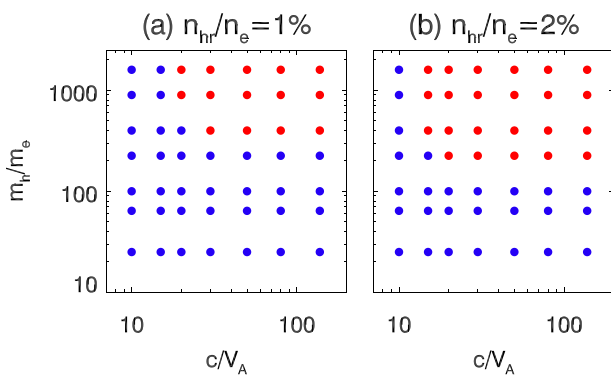


FIG. 5. The spectral properties of the excited magnetosonic waves at different ratios of the light speed to the Alfvén speed  $c/V_A$  and mass ratios of proton to electron  $m_h/m_e$  for (a)  $n_{hr}/n_e = 1\%$ , and for (b)  $n_{hr}/n_e = 2\%$ , while  $V_R$  is kept as  $1.0V_A$ . Each dot denotes one case. The red and blue colors represent a continuous spectrum and a discrete spectrum of magnetosonic waves, respectively.

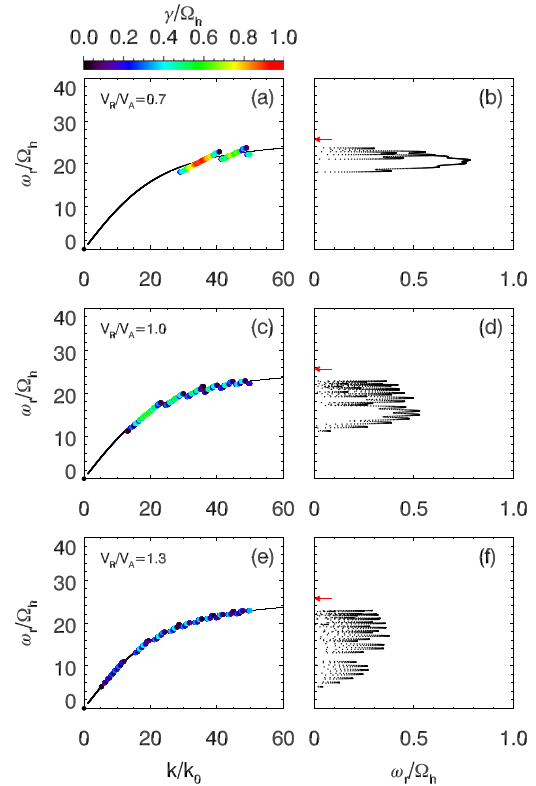


FIG. 6. (a) The normalized wave frequency  $\omega_r/\Omega_h$  versus the normalized wave number  $k/k_0$ , and (b) the normalized wave frequency  $\omega_r/\Omega_h$  versus the normalized growth rate  $\gamma/\Omega_h$  for case 11, while (c) and (d) for case 12, and (e) and (f) for case 13. The black lines in left panel represent the cold plasma dispersion relation. Colored line segments denote unstable wave modes, with red for greater  $\gamma$  and blue for smaller  $\gamma$  values. The red arrows in right panels mark the lower hybrid frequency.

Figure 6 plots the dispersion relation of perpendicular magnetosonic waves for different proton ring velocities (cases 11–13), while  $c/V_A = 50$ ,  $m_h/m_e = 900$ , and  $n_{hr}/n_e = 0.5\%$  are kept. Figure 6(a) shows the normalized wave frequency  $\omega_r/\Omega_h$  versus the normalized wave number  $k/k_0$  (left panels), and Figure 6(b) presents the normalized wave frequency  $\omega_r/\Omega_h$  versus the normalized growth rate  $\gamma/\Omega_h$  (right panels) for  $V_R = 0.7V_A$ , Figures 6(c) and 6(d) for  $V_R = 1.0V_A$ , and

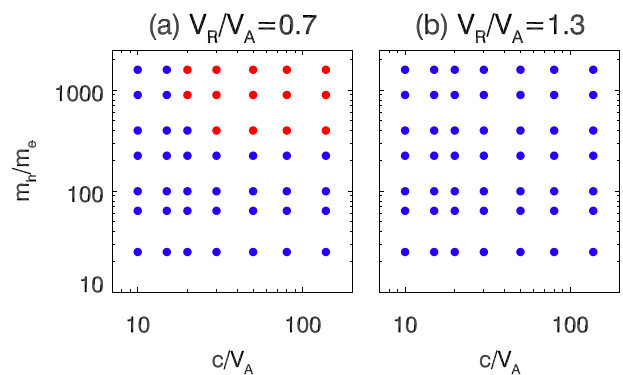


FIG. 7. The spectral properties of the excited magnetosonic waves at different ratios of the light speed to the Alfvén speed  $c/V_A$  and mass ratios of proton to electron  $m_h/m_e$  for (a)  $V_R = 0.7V_A$  and for (b)  $V_R = 1.3V_A$ , while  $n_{hr}/n_e$  is kept as  $0.5\%$ . Each dot denotes one case. The red and blue colors represent a continuous spectrum and a discrete spectrum of magnetosonic waves, respectively.

Figures 6(e) and 6(f) for  $V_R = 1.3V_A$ . With the increase of the proton ring velocity, more and more wave modes become unstable, and the spectral range of the excited modes becomes broader and broader. However, their growth rates become smaller, and the spectrum changes from a continuous structure to a discrete one with the increase of the proton ring velocity. Figure 7 exhibits the spectral properties of the excited magnetosonic waves at different ratios of the light speed to the Alfvén speed and mass ratios of proton to electron. In Fig. 7(a),  $V_R = 0.7V_A$ , and in Fig. 7(b),  $V_R = 1.3V_A$ , while  $n_{hr}/n_e$  is kept as 0.5%. Compared with Fig. 3, where  $V_R = 1.0V_A$ , we also find that the proton ring velocity cannot be too large in order to form a continuous spectrum. When  $V_R = 1.3V_A$ , a continuous spectrum cannot be formed no matter how we enlarge the mass ratio and the light speed.

#### IV. CONCLUSIONS AND DISCUSSION

In this paper, we investigate the properties of the excited perpendicular magnetosonic waves under different plasma conditions with the linear theory. The conclusions are summarized as follows:

- (1) A tenuous proton ring distribution is unstable to perpendicular magnetosonic waves. When the proton to electron mass ratio or the ratio of the light speed to the Alfvén speed is small, the excited magnetosonic waves are prone to having a discrete spectrum with only several wave modes. With the increase of the proton to electron mass ratio or the ratio of the light speed to the Alfvén speed, both the frequency and growth rate increase, and the spectrum of the excited waves becomes broader. Moreover, a continuous spectrum may be formed due to the merging of growth rate peaks when the proton to electron mass ratio and the ratio of the light speed to the Alfvén speed are sufficiently large.
- (2) The increase of the density of the ring distribution protons can enhance the growth rate of the excited waves while the frequencies nearly keep unchanged, and then a continuous spectrum is easier to be formed.
- (3) The increase of the proton ring velocity tends to increase the number of unstable wave modes. Although the spectrum of magnetosonic waves becomes broader, the growth rate of the excited wave modes becomes smaller, and the spectrum may change from a continuous structure to a discrete one.

In PIC simulations of magnetosonic waves, the reduced ratios of the proton mass to electron mass and the light speed to Alfvén speed are usually used,<sup>24</sup> and our theoretical calculations have shown that this will cause the spectral properties of the excited magnetosonic waves to change significantly. Therefore, the ratio of the proton mass to electron mass and the light speed to Alfvén speed should be chosen carefully in PIC simulations of magnetosonic waves. In the Earth's magnetosphere, the plasma parameters are quite variable, which are closely dependent on the location and the level of geoactivity. Therefore, we have considered a broad range of plasma parameters (such as  $n_{hr}/n_e$  and  $V_R/V_A$ ) in this study. It is worth noting that the cold plasma density and magnetic

field used here may be smaller than the typical values near the plasmopause (i.e.,  $B_0 \sim 100\text{--}500$  nT and  $n_e \sim 20\text{--}60$  cm<sup>-3</sup>). However, all the relevant plasma parameters in this study have already been normalized by the background plasma parameters, so the conclusions should have generality.

Recently, Chen<sup>25</sup> has studied the effects of the wave normal angle on the spectral structure of magnetosonic waves using the linear theory. In his paper, he used two subtracted Maxwellian distributions to assume a ring velocity distribution, which provides lower growth rates than an ideal ring velocity distribution (used here) if the same  $n_{hr}/n_e$  is chosen. This is why he got narrow spectral peaks at harmonics for the perpendicular wave normal angle (Figure 1 in Chen's paper).

In Paper II,<sup>26</sup> we will study the excitation of magnetosonic waves with PIC simulations, and the nonlinear characteristics of these waves will also be investigated. In addition, our theoretical calculations also show that a continuous spectrum is formed due to the merging of growth rate peaks when the growth rate of magnetosonic waves is sufficiently large. This is consistent with the satellite observations of Trurutani *et al.*,<sup>10</sup> where they found that a continuous spectrum of magnetosonic waves is usually formed when their intensity is large.

#### ACKNOWLEDGMENTS

This research was supported by the National Science Foundation of China, Grant Nos. 41331067, 41474125, 11220101002, 11235009, 41174124, and 41121003, 973 Program (2013CBA01503 and 2012CB825602), and CAS Key Research Program KZZD-EW-01-4.

<sup>1</sup>C. Russell, R. Holzer, and E. Smith, *J. Geophys. Res.* **75**, 755–768, doi:10.1029/JA075i004p00755 (1970).

<sup>2</sup>S. A. Boardsen, D. Gallagher, D. Gurnett, W. Peterson, and J. Green, *J. Geophys. Res.* **97**(A10), 14967–14976, doi:10.1029/92JA00827 (1992).

<sup>3</sup>O. Santolík, J. S. Pickett, D. A. Gurnett, M. Maksimovic, and N. Cornilleau-Wehrin, *J. Geophys. Res.* **107**(A12), 1495, doi:10.1029/2001JA009159 (2002).

<sup>4</sup>Q. Ma, W. Li, R. M. Thorne, and V. Angelopoulos, *Geophys. Res. Lett.* **40**, 1895–1901, doi:10.1002/grl.50434 (2013).

<sup>5</sup>Z. Zhima, L. Chen, H. Fu, J. Cao, R. B. Horne, and G. Reeves, *J. Geophys. Res.* **42**, 9694–9701, doi:10.1002/2015GL066255 (2015).

<sup>6</sup>D. A. Gurnett, *J. Geophys. Res.* **81**(16), 2765–2770, doi:10.1029/JA081i016p02765 (1976).

<sup>7</sup>Y. Kasahara, H. Kenmochi, and I. Kimura, *Radio Sci.* **29**(4), 751–767, doi:10.1029/94RS00445 (1994).

<sup>8</sup>J. L. Posch, M. J. Engebretson, C. N. Olson, S. A. Thaller, A. W. Breneman, J. R. Wygant, S. A. Boardsen, C. A. Kletzing, C. W. Smith, and G. D. Reeves, *J. Geophys. Res.: Space Phys.* **120**, 6230–6257 (2015).

<sup>9</sup>O. Santolík, F. Němec, K. Gereová, E. Macúšová, Y. de Conchy, and N. Cornilleau-Wehrin, *Ann. Geophys.* **22**, 2587–2595 (2004).

<sup>10</sup>B. T. Trurutani, B. J. Falkowski, J. S. Pickett, O. P. Verkhoglyadova, O. Santolík, and G. S. Lakhina, *J. Geophys. Res.: Space Phys.* **119**, 964–977 (2014).

<sup>11</sup>H. Fu, J. Cao, Z. Zhima, Y. V. Khotyaintsev, V. Angelopoulos, O. Santolík, Y. Omura, U. Taubenschuss, L. Chen, and S. Huang, *Geophys. Res. Lett.* **41**, 7419–7426, doi:10.1002/2014GL061867 (2014).

<sup>12</sup>S. A. Boardsen, G. B. Hospodarsky, C. A. Kletzing, R. F. Pfaff, W. S. Kurth, J. R. Wygant, and E. A. MacDonald, *Geophys. Res. Lett.* **41**, 8161–8168, doi:10.1002/2014GL062020 (2014).

<sup>13</sup>M. A. Balikhin, Y. Y. Shprits, S. N. Walker, L. Chen, N. Cornilleau-Wehrin, I. Dandouras, O. Santolík, C. Carr, K. H. Yearby, and B. Weiss, *Nat. Commun.* **6**, 7703 (2015).

- <sup>14</sup>R. B. Horne and R. M. Thorne, *Geophys. Res. Lett.* **25**(15), 3011–3014, doi:10.1029/98GL01002 (1998).
- <sup>15</sup>R. B. Horne, R. M. Thorne, S. A. Glauert, N. P. Meredith, D. Pokhotelov, and O. Santolík, *Geophys. Res. Lett.* **34**, L17107, doi:10.1029/2007GL030267 (2007).
- <sup>16</sup>S. Perraut, A. Roux, P. Robert, R. Gendrin, J.-A. Sauvaud, J.-M. Bosqued, G. Kremser, and A. Korth, *J. Geophys. Res.* **87**(A8), 6219–6236, doi:10.1029/JA087iA08p06219 (1982).
- <sup>17</sup>N. P. Meredith, R. B. Horne, and R. R. Anderson, *J. Geophys. Res.* **113**, A06213, doi:10.1029/2007JA012975 (2008).
- <sup>18</sup>Q. Ma, W. Li, L. Chen, R. M. Thorne, and V. Angelopoulos, *J. Geophys. Res.: Space Phys.* **119**, 844–852 (2014).
- <sup>19</sup>A. V. Gul’elmi, B. I. Klaine, and A. S. Potapov, *Planet. Space Sci.* **23**, 279–286 (1975).
- <sup>20</sup>S. A. Curtis and C. S. Wu, *J. Geophys. Res.* **84**(A6), 2597–2607, doi:10.1029/JA084iA06p02597 (1979).
- <sup>21</sup>K. McClements, R. Dendy, and C. Lashmore-Davies, *J. Geophys. Res.* **99**(A12), 23685–23693, doi:10.1029/94JA01979 (1994).
- <sup>22</sup>L. Chen, R. M. Thorne, V. K. Jordanova, and R. B. Horne, *J. Geophys. Res.* **115**, A11222, doi:10.1029/2010JA015707 (2010).
- <sup>23</sup>S. P. Gary, K. Liu, D. Winske, and R. E. Denton, *J. Geophys. Res.* **115**, A12209, doi:10.1029/2010JA015965 (2010).
- <sup>24</sup>K. Liu, S. P. Gary, and D. Winske, *J. Geophys. Res.* **116**, A07212, doi:10.1029/2010JA016372 (2011).
- <sup>25</sup>L. Chen, *Geophys. Res. Lett.* **42**, 4709–4715, doi:10.1002/2015GL064237 (2015).
- <sup>26</sup>J. Sun, X. Gao, Q. Lu, L. Chen, X. Tao, and S. Wang, *Phys. Plasmas* **23**, 022902 (2016).